J Mater Sci (2009) 44:6553–6562
DOI 10.1007/s10853-009-3612-7

MESOSTRUCTURED MATERIALS

Synthesis of ordered mesoporous Pd/carbon catalyst with bimodal pores and its application in water-mediated Ullmann coupling reaction of chlorobenzene

Haiyan Wang · Ying Wan

Received: 27 November 2008 / Accepted: 16 May 2009 / Published online: 9 June 2009

Abstract Heterogeneous palladium catalysts have been supported on the ordered mesoporous carbons (Pd/OMC) with bimodal pores which are prepared by the surfactant-templating approach. Characterization using XRD, TEM, XPS, H_2 chemisorption, and N_2 sorption techniques reveals that the Pd/OMC catalysts have the ordered 2-D hexagonal mesostructure (space group of *p6mm*), extremely high surface areas ($\sim$1800 m^2/g), large pore volumes ($\sim$1.64 cm^3/g), bimodal pores (6.3 nm of primary mesopores and 1.7 nm of secondary mesopores inside the pore walls), hydrophobic carbon surface, and small metal particles well-dispersed inside the secondary small mesopores. This catalyst exhibits a high yield of 43% for biphenyl from the Ullmann coupling reaction of chlorobenzene in water at 100 °C without assistance of any phase transfer catalyst and can be reused up to 10 times, providing potential opportunities for industrial applications such as coupling and hydrogenation reactions.

Introduction

Supported palladium/activated carbons are frequently used heterogeneous catalysts in hydrogenation and coupling reactions [1–3]. Activated carbons are prepared by chemical and physical activation processes. They have broad pore-size distributions, ranging from micropores to macropores. This phenomenon may lead to a non-uniform distribution of metal active sites, limit their applications, and fail to establish the relationship between the pore texture/surface nature/metal size of catalysts, and the catalytic performance [4, 5]. Ordered mesoporous carbons (OMCs) possess well-controlled pore structures, high surface areas, and large and tunable pore sizes [5–15]. These characters facilitate the studies of the influence by the pore texture and metal size on catalytic activity. The synthesis of OMCs includes the nanocasting and surfactant-self-assembly approaches [5–15]. The self-assembly route is a facile method [11–15]. For example, highly OMCs with tunable pore sizes can be produced in batch using cheap, soluble phenolic resins as carbon precursors, and commercially available triblock copolymer as a structure-directing agent [13]. Up to now, no studies have been published on the catalytic behaviors of mesoporous carbons derived from the surfactant self-assembly route.

The biaryl structure is important in many dye chemicals, pharmaceutically relevant, and biologically active compounds. Ullmann coupling reaction of halobenzene is one of the main ways for the synthesis of symmetrical biaryls [16–18]. Supported palladium on carbon and mesoporous silica carriers have been used to replace conventional copper catalyst in recent years [16, 19, 20]. However, the reactions are usually carried out under rigorous conditions, for example, high temperature, the presence of organic solvent such as *N,N*-dimethylformate or toluene and/or phase transfer catalyst including crown ether [17], polyethylene glycol [18], etc. Although mild conditions (air and room temperature) were adopted and high yields of biphenyl were achieved, only iodo- and bromobenzene could be used as reactants [17]. From the viewpoint of the environmentally benign organic reactions, water-containing media is popular due to reduction of burden by organic solvent disposal [21–26]. Chlorobenzene is cheaper and more common than iodobenzene and bromobenzene, being

H. Wang · Y. Wan (✉)
Department of Chemistry, Shanghai Normal University, Shanghai 200234, People's Republic of China
e-mail: ywan@shnu.edu.cn

more valuable in the coupling reaction; and on the other hand, Cl-containing organic compounds are one of the most serious contaminants in water. The coupling reaction or the dehydrochlorination is difficult because of high energy of C–Cl bonds [27, 28]. Therefore, developing new catalysts that allow the Ullmann coupling reaction of chlorobenzene conducted at room temperature in aqueous media is important for both economic and environmental concerns.

Here, we report the water-mediated Ullmann coupling reactions of chloroenzene over the heterogeneous bimodal palladium catalysts which are supported on OMCs. The OMCs are produced on the basis of triblock-copolymer-templating approach, possessing the 2-D hexagonal mesostructure, extremely high surface areas ($\sim$2200 m^2/g), large pore volumes ($\sim$1.89 cm^3/g), and uniform bimodal pores (6.3 nm of primary mesopores and 1.7 nm of secondary mesopores inside the pore walls). After impregnation, the well-ordered mesopore structure (the space group of *p6mm*) and bimodal pores (6.3 and 1.7 nm) can be retained, and the BET surface areas ($\sim$1800 m^2/g) and total pore volumes (1.64 cm^3/g) only show a slight decrease. Metallic Pd nanoparticles with a size about 2-nm are well-dispersed inside secondary pores. The novel Pd catalyst exhibits a yield of 43% for biphenyl at 100 °C and can be reused more than 10 times, providing a mild, economic, and green route for the synthesis of symmetrical biaryls.

Experimental section

Catalyst preparation

Ordered mesoporous carbons (OMCs) were synthesized by using soluble phenolic resins as precursors and triblock copolymer F127 as a structure-directing agent, according to an established procedure [29]. Soluble phenolic resins were prepared by the base-catalyzed polymerization of phenol and formaldehyde [13]. A typical synthesis is as follows: 2.08 g of TEOS were pre-hydrolyzed in the presence of 1.0 g of HCl (0.2 M) and 8.0 g of ethanol. The mixture was then added to the solution containing 1.0 g of preformed phenolic resin (polymerized by 0.61 g phenol and 0.39 g formaldehyde), 1.6 g of F127, and 8.0 g of ethanol. Then, the solution was poured into several dishes. After ethanol evaporation at room temperature for 8 h and thermopolymerization at 100 °C for 24 h, the membranes were scratched from the dishes. The as-made sample was then heated at 350 °C for 5 h to remove the triblock copolymer and at 900 °C for 4 h to carbonize under nitrogen. The ordered mesoporous silica–carbon (OMSC) nanocomposite was obtained. Ordered mesoporous carbon (OMC) was recovered after immersion of the mesoporous carbon–silica nanocomposite in 10% HF solution to dissolve the silica component, filtration, washing with water. and drying at 100 °C.

Supported palladium catalysts were prepared by isochoric impregnation. In a typical procedure, 0.8 g of an aqueous solution of $PdCl_2$ (1.1 wt%) was impregnated with 0.1 g of dry OMC carrier. The mixture was placed in a hood overnight. Then, the catalyst was dried at 100 °C under vacuum, reduced at 200 °C in forming gas (10 vol% H_2 in nitrogen) for 3 h, and named as fresh supported catalyst (Pd/OMC).

For comparison, a special mesoporous activated carbon was also used as a carrier to support Pd (Pd/AC) with the same Pd content and by the same isochoric impregnation procedure. Activated carbon was supplied by Xinzhuang activated carbon Company of Shanghai. Before use, it was boiled in hot KOH solution (10 wt%) at 100 °C for about 4 h, and the treatment was repeated five times. Finally, the carbon powders were calcined at 900 °C for 4 h under nitrogen.

Characterization

The X-ray diffraction (XRD) measurements were taken on a Rigaku Dmax-3C diffractometer using Cu Kα radiation (40 kV, 30 and 40 mA, $\lambda = 0.15408$ nm). The *d*-spacing values were calculated by the formula $d = n\lambda/2\sin\theta$, and the unit cell parameters were calculated from the formula $a = 2d_{10}/\sqrt{3}$. The metallic Pd sizes were estimated according to the Scherrer formula: size $= 0.89\lambda/\beta\cos\theta$ on the basis of the 111 diffraction peak in wide-angle XRD patterns. N_2 adsorption–desorption isotherms were measured at 77 K with a Quantachrome NOVA 4000e analyzer. The Brunauer–Emmett–Teller (BET) method was utilized to calculate the specific surface areas (S_{BET}). With the use of the Barrett–Joyner–Halenda (BJH) model, the pore volumes and pore size distributions were derived from the adsorption branches of isotherms. The total pore volumes, V_t, were estimated from the adsorped amount at a relative pressure p/p_0 of 0.99. The micropore volumns (V_{micro}) and micropore surface areas (S_{BET}^{micro}) were calculated from the *V-t* plot method. The *t* values were calculated as a function of the relative pressure using the de Boer equation, $t/\text{Å} = [13.99/(\log(p_0/p) + 0.0340)]^{1/2}$. V_{micro} were obtained using the equation $V_{micro}/cm^3 = 0.001547I$, where *I* represents the *Y* intercept in the *V-t* plot. Transmission electron microscopy (TEM) experiments were conducted on a JEM 2100 microscope operated at 200 kV. Energy dispersive X-ray spectroscopy (EDX) was performed on a Philips EDX instrument. Thermal gravity analysis (TGA) curves were monitored on a Mettler Toledo 851e apparatus. X-ray photoelectron spectroscopy (XPS)

measurements were performed on a Perkin–Elmer PHI 5000CESCA system with a base pressure of 10^{-9} Torr. The Pd-loading on the carriers was determined by the inductively coupled plasma-atomic emission spectrometry (ICP-AES, Varian VISTA-MPX). H_2 chemsorption tests were conducted on a Quantachrome CHEMBET-3000 system by pulsing hydrogen on the supported Pd catalysts. Palladium surface areas were calculated from H_2 chemisorption data assuming that all the palladium particles were spherical and that the adsorption stoichiometry was one H atom per Pd metal [30]. The metal surface areas (S_{Pd}) were given by the formula: $S_{Pd} = 18.5V_{ads}N_0/22.4 \times 10^{20} \times$ metal content (wt%) (here, the value 18.5 is the surface area of one molecule of H_2 and V_{ads} is the volume of H_2 chemisorbed). The palladium sizes were estimated according to the formula: $d = 5/\rho_{Pd}S_{Pd}$.

Activity test

The Ullmann coupling reactions were carried out in a 50-mL round-bottled flask with refluxing by using chlorobenzene as the reactant and water as the solvent. In a typical reaction, 1.0 g of chlorobenzene, 10 mL of water, 2.2 g of sodium formate, 2.8 g of potassium hydroxide, and 0.1 g of supported palladium catalyst were charged to the vessel. The reaction temperature was adjusted between 30 °C and 100 °C. After 6-h stirring, the products were centrifuged, extracted with toluene, and analyzed by a gas chromatograph (Agilent 1790) equipped with a JW DB-5, 95% dimethyl 1-(5%)-diphenylpolysiloxane column and a FID detector. The column temperature was programmed from 100 °C to 250 °C at the ramp speed of 10 °C min^{-1}. After the reaction, the catalyst Pd/OMC was separated, washed with toluene and water, and then dried under vacuum. It was then reused with fresh solvent and reactants for further runs with the same reaction conditions maintained.

Results and discussion

The synthesis of mesoporous carbon is on the basis of triconstituent co-assembly approach using triblock copolymer F127 as a structure-directing agent, and soluble phenolic resins and TEOS as sources [29]. First, the ordered mesoporous silica–carbon (OMSC) composite is obtained. The TG curve for OMSC which is carried out in air shows two distinct weight losses of 6% and 42% in the range of 50–200 °C and 300–700 °C, attributed to the removal of physisorbed water and organic solvent, and carbon in the framework, respectively (Fig. 1). The carbon and silica components are therefore in a weight ratio of 1:1.2. The OMC product is a derivation of OMSC upon dissolving silica by HF. A complete weight loss is observed in the TG curve for the OMC sample, and no ash component is residual after heating the sample from 100 °C to 700 °C in air, indicating the pure carbon composition in OMC. The EDX pattern also reveals the absence of Si in the carbon containing OMC. Supported palladium catalysts were prepared by isochoric impregnation of OMC with an aqueous solution of $PdCl_2$ and subsequent reduction. The palladium content is about 5 wt%, measured by ICP-AES.

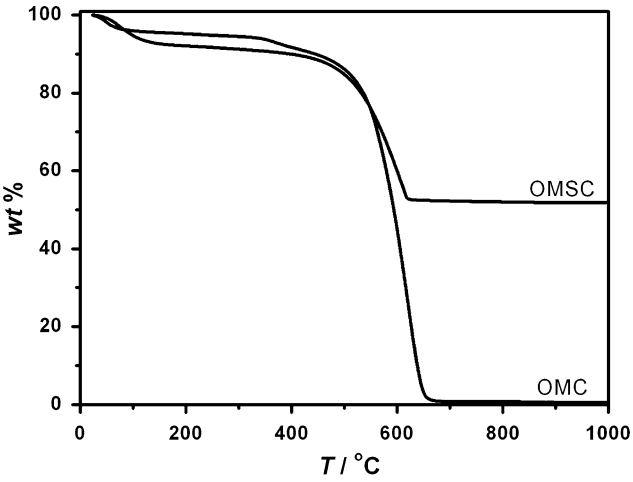

Fig. 1 TG curves of the ordered mesoporous carbon–silica nanocomposite (OMSC) and the ordered mesoporous carbon (OMC). The curves were taken from room temperature to 1000 °C with a ramp rate of 10 °C/min in air

The small-angle XRD patterns for OMSC, OMC, and Pd/OMC are shown in Fig. 2a. Three well-resolved diffraction peaks in the 2θ range of 0.5–2° are observed for the OMSC composite after carbonization at 900 °C. The *d*-value ratios are $1:\sqrt{3}:2$, indicating a highly ordered 2-D hexagonal mesostructure (space group: *p6mm*). The cell parameter is calculated to be 11.9 nm (Table 1). Because the two components in the silica–carbon composite, namely silica from TEOS and carbon from phenolic resins, have distinct difference in the framework shrinkage between the as-made materials and the final products (silica of 42% and carbon of 80%), the cell parameter would not be clearly identified if the macrophase separation of silica and carbon occurs. Therefore, in the present case, the carbon and silica components are homogenously dispersed inside the same composite framework [29]. The strong 10 diffraction at 2θ of 0.86° is retained for the carbon material after removal of silica in OMSC, which is corresponding to a repeated unit of 11.8 nm, almost the same as the mother OMSC. The peaks at higher angles between 1.5° and 1.7° become diffused. These results indicate the maintenance of the mesostructure upon dissolving the silica component and the well dispersion of silica and carbon inside the composite framework. After incorporation of Pd on OMC, the XRD pattern is similar to the pure carbon carrier, the

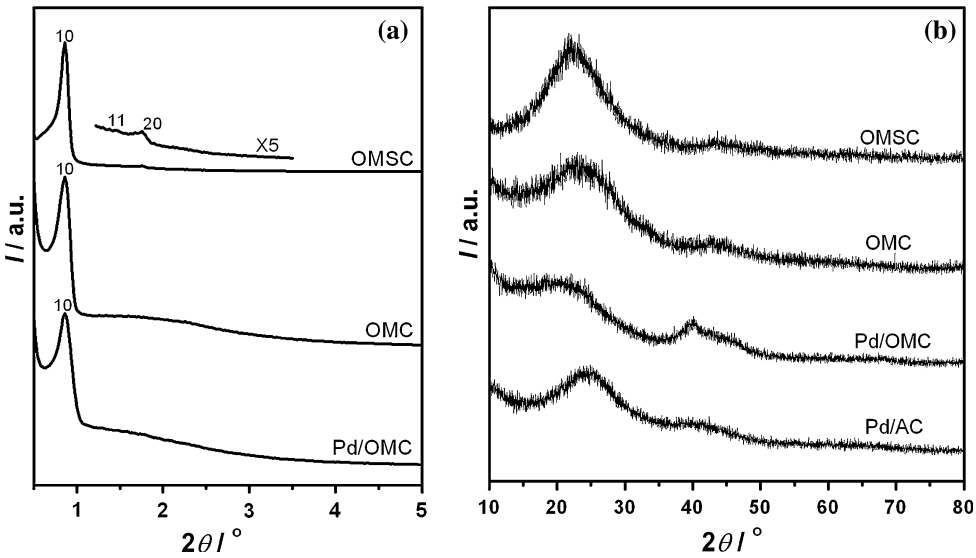

Fig. 2 Small-angle XRD patterns (**a**) and wide-angle XRD patterns (**b**) of the ordered mesoporous carbon-silica (OMSC) nanocomposite, the ordered mesoporous carbon (OMC), the ordered mesoporous supported palladium (Pd/OMC) catalyst, and the activated carbon supported palladium (Pd/AC) catalyst

Table 1 Physical properties of ordered mesoporous silica–carbon (OMSC) nanocomposite, ordered mesoporous carbon (OMC), ordered mesoporous Pd/OMC catalyst—this catalyst after 5 catalytic Ullmann reaction runs Pd/OMC-5run, mesoporous activated carbon carrier (AC), and Pd/AC catalyst

Sample	a_0 (nm)	S_{BET} (m^2/g)	D_P (nm)	V_t (cm^3/g)	V_{micro} (cm^3/g)
OMSC	11.9	398	6.3	0.51	0.04
OMC	11.8	2249	6.3/1.7	1.89	0
Pd/OMC	11.7	1819	6.3/1.7	1.64	0
Pd/OMC-5run	11.9	1810	6.3/1.6	1.62	0
AC	–	1663	–	1.45	0
Pd/AC	–	1515	–	1.33	0

one strong together with a weak and wide peak, and the same lattice spacing. The results clearly indicate that the OMC is stable, and the highly ordered mesostructure is retained after the impregnation of metallic solution, drying, and reduction.

It is known that the phase transformation of liquid crystalline mesophases is from lamellar to bicontinuous cubic, hexagonal, and body-centered cubic as the hydrophilic–hydrophobic balance number (n_H/n_L) grows. The main silica product in the F127-template system with a large PEO/PPO ratio is the cubic mesostructure with the $Im\bar{3}m$ symmetry [31]. In fact, the prediction is rough due to the fact that the n_H/n_L value is contributed from the silicate/triblock copolymer composite. The composite has a continuously changeable n_H/n_L value caused by the condensation of silica species. When phenolic resins are adopted as precursors, the polymeric framework remains unchanged without polymerization during self-assembly under neutral condition and room temperature. At that time, the hydrophobic and hydrophilic volume ratio of the phenolic resin/triblock copolymer is a constant. It is, therefore, necessary to tune the n_H/n_L value in a wide range. A low ratio of phenol/F127 yields a 2-D hexagonal mesostructure of carbon, and a high ratio leads to a cubic mesostructure [32]. Therefore, the formation of the 2-D hexagonal mesostructure templated by the triblock copolymer F127 can be attributed to the adjustment of the n_H/n_L value by phenolic resins, despite the presence of TEOS.

Representative TEM images for the mesoporous silica–carbon, the mesoporous carbon carrier, and the supported Pd catalyst show typical hexagonally arranged and stripe-like pores, confirming the 2-D hexagonal mesostructure (Fig. 3). The TEM images for OMSC are uniform in large domains with the same cell parameter, and the EDX patterns reveal that carbon and silica are presented and well dispersed in the same particle, suggesting that the pore wall is composed of silica and carbon. Although the XRD diffraction peaks in the range of 1.5–2° for OMC are not as resolved as the mother OMSC, TEM images exhibit the ordered mesostructure in large domains. No distinct defect is observed. The estimated cell parameter is similar to that of OMSC, further demonstrating that the removal of silica in OMSC has negligible effect on the mesostructure. The incorporation of metallic Pd also leads to a minor change on the mesostructure, as evidenced by the similar TEM images with the same spacing lattice as the OMC carrier. This phenomenon implies the stable mesostructure. It is very interesting to note that Pd aggregates cannot be observed in the TEM images for the Pd/OMC catalyst. Only small particles can be found inside the carbon pore walls (circles in Fig. 3f). The EDX pattern clearly reflects the presence of Pd. A careful analysis by mapping the image reveals the very good distribution of Pd nanoparticles in the whole carbon particle (data not shown).

The XPS spectrum of the supported Pd catalyst (Pd/OMC) (Fig. 4) shows two peaks with the binding energy at

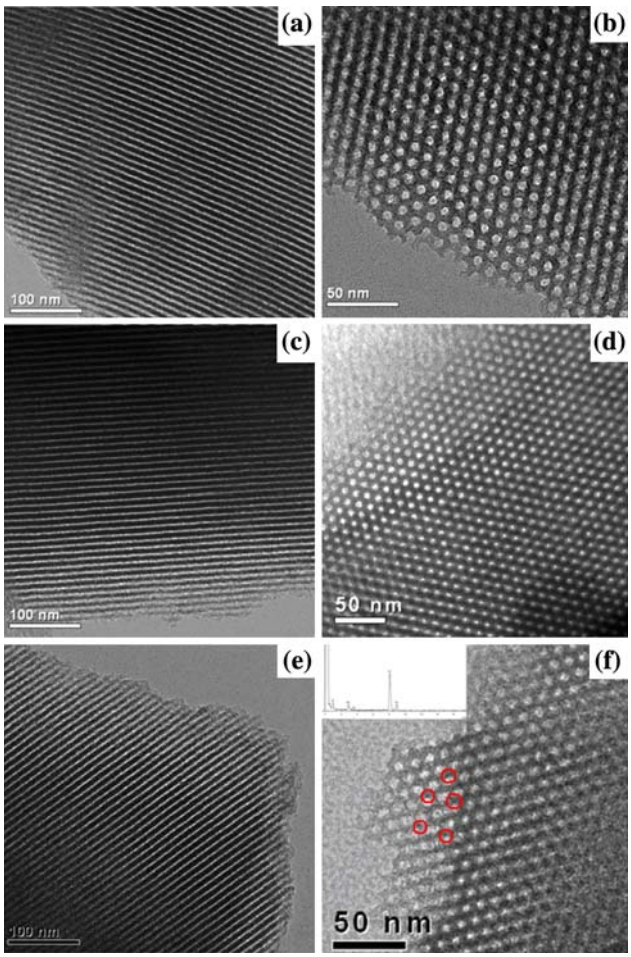

Fig. 3 TEM images of OMSC (**a** and **b**), OMC (**c** and **d**), and Pd/OMC (**e** and **f**), recorded along the [100] (**a**, **c,** and **e**) and [001] (**b**, **d,** and **f**) directions. Inset f is the EDX pattern

around 340.8 and 335.1 eV, corresponding to Pd(0) in the $3d_{3/2}$ and $3d_{5/2}$ level [33], indicating that the Pd species in the catalyst Pd/OMC present in the metallic state. The wide-angle XRD patterns of OMC displays one diffraction shoulder at $2\theta \sim 25°$ together and a broad diffraction peak at about 42°, corresponding to the 002 and 10 reflections of amorphous carbon materials. After impregnation of Pd ions and subsequent reduction, three diffraction peaks appear at 2θ of 40.1, 46.5, and 68.0°. These three diffractions can be attributed to the 111, 200, and 220 reflections of the face-centered cubic (*fcc*) Pd lattice, proving the reduction of metallic Pd. However, the intensities are relatively low and the peaks are wide, possibly owing to the small particle size and very good dispersion of metal in the carbon framework. Estimation on the basis of the Scherrer formula gives the particle size of about 2.1 nm. This estimation is rough due to the fact that the diffraction peak of the 111 reflection for metallic Pd is wide and weak, as well as overlaps with the 10 diffraction for amorphous carbon. However, the result reflects that the particle size is very

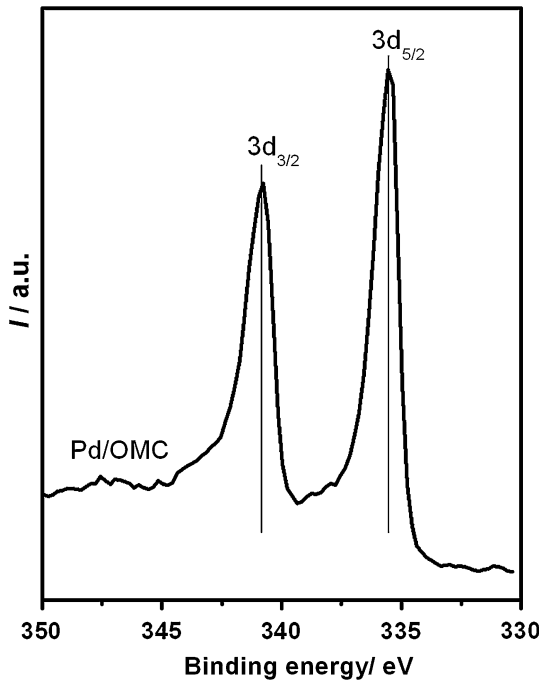

Fig. 4 XPS spectrum of the palladium catalyst supported on ordered mesoporous carbon (Pd/OMC)

small, confirming the TEM results. The H_2 chemisorption measurement reveals that the metallic Pd size is 2.4 nm, and the specific surface area is 174 m^2/g, which are in good agreement with the XRD and TEM results.

The OMSC, OMC, and Pd/OMC show the type-IV shape of nitrogen adsorption isotherms (Fig. 5), characteristic for nanostructured materials with uniform mesopores. The BET surface area, pore volume, and pore size of OMSC is 398 m^2/g, 0.51 cm^3/g, and 6.3 nm, respectively (Table 1). The *t*-plot analysis reflects that this sample has a micropore surface area of 71 m^2/g (Fig. 6). Almost whole of the total surface areas and pore volumes are contributions due to mesopores. Remarkably, after dissolving silica, the OMC carrier possesses an extremely high BET surface area of 2249 m^2/g, a pore volume of 1.89 cm^3/g, and a bimodal pore-size distribution with the most probable pore sizes of 6.4–1.7 nm. The primary mesopore size is the same as its mother OMSC, while the secondary one is much smaller (1.7 nm). A distinctly increased adsorption at relative pressures of p/p_0 of 0.1–0.3 is indeed observed for OMC (Fig. 5), suggesting small pores below 3.0 nm. The micropores (below 1.5 nm) surface area is negligible on the basis of the *t*-plot analysis (Fig. 6), the primary mesopores (6.3 nm) surface area is 398 m^2/g, and the volume is 0.51 cm^3/g inherent from the mother OMSC with the same primary mesopores. Therefore, the secondary mesopores contribute to 85% in surface area and pore volume. Though the practical condition is more complicated because of the different densities of the carbon and silica components

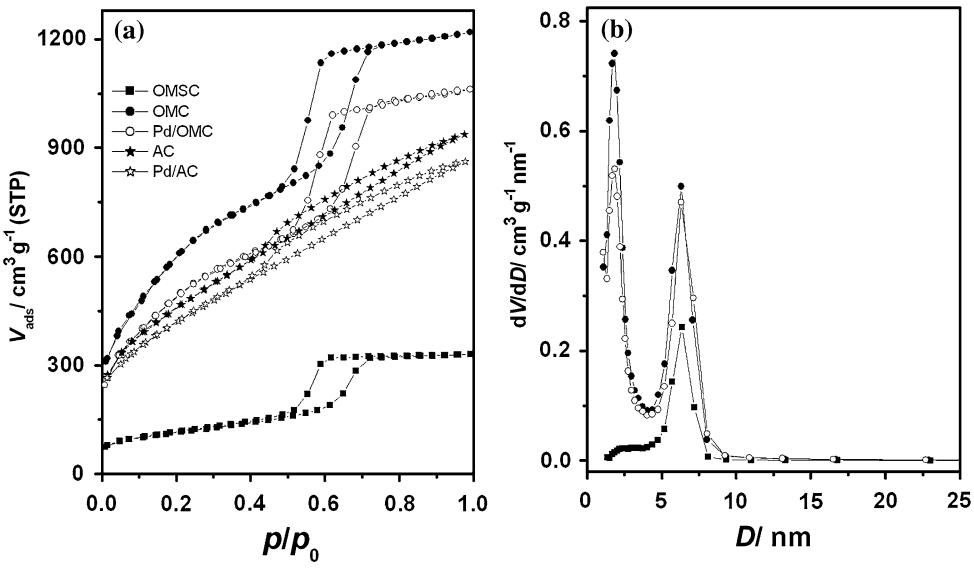

Fig. 5 Nitrogen sorption isotherms (**a**) and pore-size distribution curves (**b**) of OMSC, OMC, AC, Pd/OMC, and Pd/AC

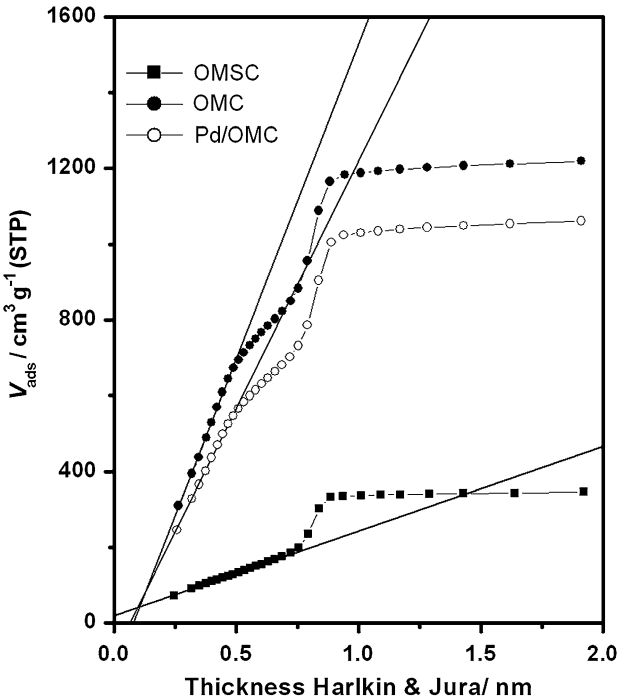

Fig. 6 *V-t* plots for the ordered mesoporous silica–carbon (OMSC) composite, the mesoporous carbon carrier (OMC), and the supported Pd catalyst (Pd/OMC)

(amorphous carbon: 1.8–2.1 g/cm^3 and amorphous silica: 2.2–2.6 g/cm^3), the estimation can reflect the fact that lots of voids are appearing in the pore walls and that these secondary mesopores inside pore walls contribute to the majority of the total pore surface area and volume. The negligible micropores and large-amount secondary mesopores in OMC upon dissolution of silica in OMSC have also been reported by Liu et al. [29]. The OMC with bimodal mesopores is derived from the OMSC composite, which are prepared by the triconstituent (TEOS, phenolic resol and triblock copolymer F127) co-assembly route [29]. A schematic diagram is shown in Fig. 7: (1) During the co-assembly, the phenolic resin and silica aggregate around the triblock copolymer aggregates, and the mesostructured composite is formed; (2) After high-temperature heating, triblock copolymer can be removed. Simultaneously, the silica component cross-link and polymer component get carbonized to carbon. The mesoporous solids have only primary mesopores with a size of 6.3 nm, the pore wall of which is composed by silica and carbon. Therefore, the primary mesopores are generated by removal of triblock copolymer; (3) Subsequently, the silica–carbon composite was etched by HF solution. As a result, the silica component is eliminated and the carbon component is left. The mesostructure can be well retained and the primary mesopores keep unchanged. However, lots of voids are generated inside pore walls. Therefore, the primary mesopores are inherited from the mother, and the secondary small mesopores are more likely generated by the removal of silica component in the carbonaceous framework. The mild treatment by 10% HF solution shows an insignificant effect on the primary mesopores and the mesostructure, with only plenty of voids being left inside the framework. These secondary mesopores are interpenetrated and accessible due to the fact that the silica and carbon components are well dispersed inside the whole framework, and contribute to the majority of pore surface areas and volumes.

After incorporation of Pd, the shapes for nitrogen sorption isotherms of OMC and Pd/OMC and the capillary condensation step ranging from 0.5 to 0.7 remain almost unchanged, implying a minor change in the mesopore volume. The pore-size distribution curves reveal that both the primary and secondary mesopores sizes are similar. The

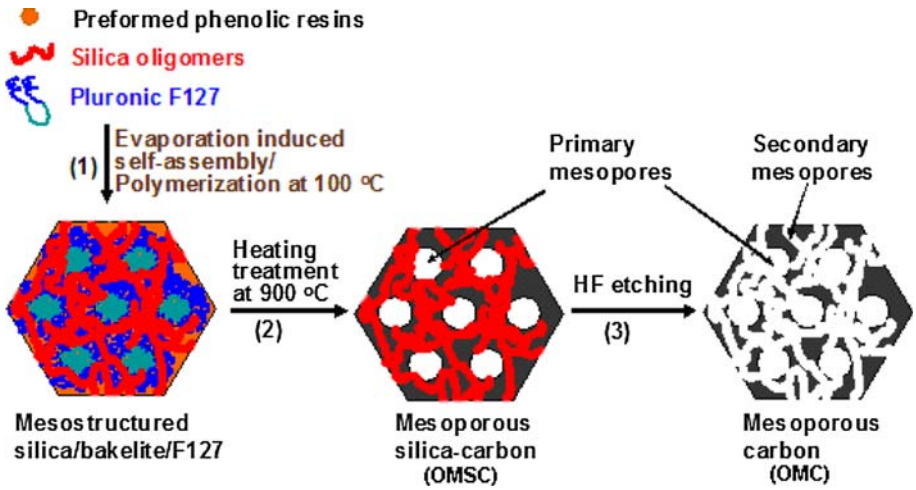

Fig. 7 Scheme for the generation of secondary mesopores in the OMC carrier: (1) Evaporation-induced triconstituent co-assembly of TEOS, phenolic resin, and triblock copolymer F127, and low-temperature polymerization at 100 °C to form mesostructured silica/bakelite/triblock copolymer composite. (2) Heating treatment at 900 °C to remove template, cross-link silica, and carbonize carbon. Primary mesopores, which resulted from the elimination of the triblock copolymer template, are open in this stage, and the pore wall is constructed by carbon and silica in the OMSC nanocomposite; (3) HF etching to remove the silica component. Secondary mesopores inside pore walls are generated in the final product, OMC

difference lies in the low pressure range of $p/p_0 = 0.1$–0.3. A lower adsorbed volume is detected for Pd/OMC than OMC, indicating the decrease of pore volume in the secondary mesopores. Accordingly, the BET surface area and pore volume reduces to 1819 m^2/g and 1.64 cm^3/g, respectively. These results, together with the above TEM, XRD, and H_2-chemisoprtion analysis, indicate that the small particles locate inside the secondary mesopores and may block some pores.

It is interesting to note that the Pd nanoparticles are predominantly involved in the secondary mesopores. The incipient or wetness impregnation has been widely used to introduce metals or metal oxides inside mesopores. For example, with the use of mesoporous silica SBA-15 as a hard template and $Pt[(NH_3)_4](NO_3)_2$ as a precursor, Stucky and co-workers synthesized noble metal nanowires [34]. Lots of secondary mesopores locate inside the SBA-15 mesoporous silica pore walls to connect the two adjacent straight pore channels. Pt ions can enter into both primary and small pores and further be reduced to nanowires and short nanorods. On removal of silica, ordered mesoporous Pt nanowire arrays can be prepared, and the two nanowires are supported by Pt nanorods. The capillary force is responsible for the involvement of metallic solution inside the channels; however, the interaction between solution and pore walls of mesoporous materials is of importance for impregnation [5–10]. In the silica pores, metal solutions have interaction with silanol groups, which facilitates the distribution of metal ions inside the whole channels including the primary mesopores and secondary pores inside pore walls. The OMC carrier has uniform mesopores so that metallic solution can homogenously enter the pores. However, the carbon surface is extremely hydrophobic and has weak interaction with palladium ions. The diffusion of metallic solution into secondary mesopores inside the pore walls is predominant because of the capillary force. The involvement of adsorbate inside the secondary small pores of mesoporous carbons has also been reported in the adsorption of metallic solution and dye molecules [35, 36]. On reduction, the Pd nanoparticles are formed in the confined space or, at the orifice of these secondary mesopores. Different from the silica surface with plenty of silanol group which facilitates the immobility of metal during reduction and the aggregation of metal, carbon has inert surface which may inhibit the transportation of metal and favor the formation of nanoparticles. The reductive ability of carbon may also be responsible for the localization of Pd nanoparticles instead of aggregation. As a result, no obvious palladium nanoparticles are observed inside the primary mesopore channels in the TEM images.

The mesoporous Pd/OMC catalyst was tested on the Ullmann coupling reaction of chlorobenzene in water (Table 2). This catalyst shows the ability in activating chlorobenzene at a temperature close to room temperature (30 °C) using water as a solvent without assistance of a phase transfer catalyst. The conversion of chlorobenzene is 45%, and the selectivity to the coupling product biphenyl is 23%. The only byproduct is the dehalogenation product benzene. When the reaction temperature increases to 100 °C which is normally used for the Ullmann coupling reaction, chlorobenzene can completely convert to biphenyl (43%) and benzene (57%). After the reaction, the liquid

Table 2 Catalytic performance and recycle test for the mesoporous Pd/OMC catalyst and Pd/AC in the Ullmann coupling reaction of chlorobenzene

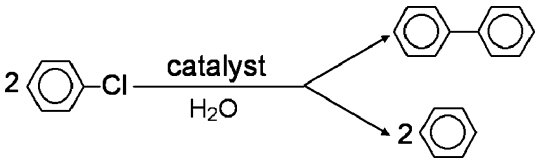

Catalyst	Reaction temperature (°C)	Cycle[a]	Conversion (%)	Selectivity (%)	
				Biphenyl	Benzene
Pd/AC	30	1	32	21	79
	100	1	59	37	63
Pd/OMC	30	1	45	23	77
	100	1	>99	43	57
	100	2	>99	38	62
	100	5	>99	40	60
	100	8	>99	42	58
	100	11	>99	40	60

[a] The Ullmann reactions are carried out using 1.0 g of chlorobenzene, 10 mL of water, 2.2 g of sodium formate, and 2.8 g of potassium hydroxide. The reaction time is 6 h. In the first run, 0.1 g of fresh supported palladium catalyst (5 wt%) is added. After reaction, the catalyst is recovered by centrifugation, washing, and drying and used in the successive runs. In the successive runs, the catalyst is weightd, and the amounts of reactants accordingly change

phase of the reaction mixture is collected by filtration and analyzed by ICP-AES. The analysis reveals the absence of Pd in the mixture, demonstrating no leaching of Pd from the solid catalyst. Therefore, the reactions undergo heterogeneous conditions, where the reactant selectively adsorb on active centers and then convert to products. Compared with our previous results [37, 38], in which 0.5 g of 6 wt% Pd/organosilica catalyst (6 times higher amount of palladium than this case) was used for the production of biphenyl from bromobenzene and iodobenzene, the present process is more efficient and economic.

The metal particle size, pore size, and pore surface of a heterogeneous catalyst show great influence on the catalytic performance. Keane et al. [39]. found that smaller palladium particles ($\leq$5 nm) exhibited intrinsically higher specific activities on the liquid-phase hydrodechlorination of 2,4-dichlorophenol over Pd/Al_2O_3 than larger metal particles. The small metal size would lead to a high active surface area, and hence, enhance the catalytic activity. In addition, Pd/functionalized mesoporous silica was found to show a better catalytic performance on converting iodo- and bromobenzene to biphenyl in aqueous solution than Pd/amorphous silica [37, 38]. The hydrophobic organic functional group inside the pore walls and uniform mesopore sizes of the mesoporous carrier is possibly responsible for the improvement. Consequently, the high catalytic performance of Pd/OMC in water may be related to the well-dispersed and small metal particles, inherent hydrophobicity of the carbon carrier, and the large, uniform mesopores. The Pd nanoparticles have high surface energy, which can activate the C–Cl bonds, the hydrophobic surface can selectively adsorb organic substrate from a large amount of water, and the uniform mesopores facilitate the mass transportation of the reactant and products.

For comparison, Pd was also supported on a special mesoporous activated carbon. The Pd/AC catalyst shows the BET surface area, pore volume, and pore size of 1515 m^2/g, 1.33 cm^3/g, and 1.5–30 nm, respectively. The high mesoporosity is considered to be good for adsorbing large molecules and can be comparable to OMC. The Pd/AC catalyst shows 32% conversion of chlorobenzene and 21% selectivity for biphenyl at 30 °C, as well as 59% conversion and 37% selectivity at 100 °C. The diffraction peaks belonging to *fcc* Pd are unresolved in the wide-angle XRD pattern for Pd/AC, implying the relatively small particle size. Therefore, the ability in activating chlorobenzene over the Pd/AC catalyst may be also due to the nanosized Pd, hydrophobic pore surface and mesopore size. However, on comparison with Pd/OMC, the Pd/AC catalyst displays a lower activity. This phenomenon is possibly related to the pore size distribution of the carrier. The mesopores are uniform in Pd/OMC, resulting in uniformly sized Pd particles because of the confined growth inside pores. In addition, the secondary mesopores which locate inside pore walls are short (normally shorter than the pore-wall thickness). The diffusion of reactants and products is

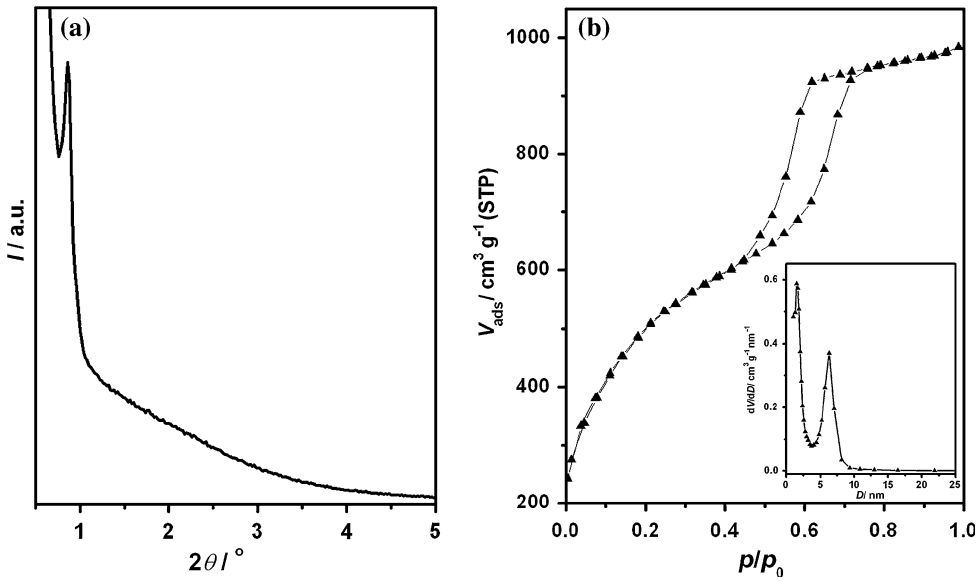

Fig. 8 Small-angle XRD patterns (**a**) and Nitrogen sorption isotherms (**b**) of Pd/OMC-5run. Pd/OMC-5run denotes the heterogeneous palladium catalyst Pd/OMC after 5 catalytic Ullmann reaction runs. Inset in **b** is the pore-size distribution curve

improved because of the short path. The AC carrier has a wide pore-size distribution, ranging from 1.5 nm to 30 nm; some small pores may easily undergo blockage where Pd grows at the orifice, causing an inhibited catalytic activity.

The mesoporous Pd/OMC catalyst was also tested for reusability. After 10 times of reuse in the Ullmann coupling reaction of chlorobenzene in water, the catalyst shows negligible loss in both conversion and selectivity (Table 2). The XRD pattern and N_2 sorption isotherms for the Pd/OMC catalyst show negligible changes after repeated use (Fig. 8). The BET surface area, pore volume, and pore sizes for Pd/OMC-5run (the catalyst after 5 catalytic runs under the same reaction conditions) are 1810 m^2/g, 1.62 cm^3/g, and bimodal 6.3/1.6 nm, respectively, almost the same as the fresh catalyst. These results indicate that this catalyst is stable in hot water. The hydrophobic surface of carbon inhibits the involvement of water inside pores. This character, together with the inert surface, suppresses the mobility of metals in the pores. As a result, negligible leaching and aggregation of Pd particles would occur even at a high temperature. This feature paves the way for the Pd/OMC catalyst in practical coupling and hydrogenation reactions.

Conclusion

Heterogeneous palladium (Pd) catalysts have been supported on OMC (OMC), and exhibit a high yield of 43% for biphenyl from the Ullmann coupling reaction of chlorobenzene in water at 100 °C without assistance of any phase transfer catalyst. The Pd/OMC catalyst is stable, showing negligible loss in activity even after a maximum of 10 catalytic recycles. The preparation of the catalyst involves the triconstituent co-assembly of TEOS, phenolic resol, and triblock copolymer, carbonization of the OMSC frameworks, etching of silica component to form OMC and impregnation of Pd inside pores (Pd/OMC). The OMSC composites have the ordered mesostructure with the space group of *p6mm*, surface areas of ~400 m^2/g, and large mesopore sizes of 6.3 nm. The dissolution of silica inside silica–carbon frameworks shows minor effect on the mesostructure and primary mesopores only leaving lots of short rods inside pore walls, and generating secondary mesopores, large surface areas, and large volumes. As a result, the Pd/OMC catalysts have the ordered 2-D hexagonal mesostructure, extremely large surface areas (~1800 m^2/g), large pore volumes (~1.64 cm^3/g), bimodal pores (6.3 and 1.7 nm), hydrophobic carbon surface, and small well-dispersed metal particles (~2 nm) inside the secondary mesopores. These unique features offer the supported Pd catalyst the ability in activating chlorobenzene in water without assistance of phase transfer catalyst. The use of OMC carrier provides a mild, economic, and green route for the synthesis of symmetrical biaryls.

Acknowledgements This work was supported by NSF of China (20873086 and 20821140537), Shanghai Sci. & Tech. and Edu. Committee (07QH14011, 07SG49, S30406, 0852nm0090 and 08JC1417100), and the program for New Century Excellent Talents in Universities (NCET-07-0560).

References

1. Balachari D, Quinn L, O'Doherty GA (1999) Tetrahedron Lett 40:4769
2. Kohler K, Heidenreich RG, Krauter JGE, Pietsch M (2002) Chem Eur J 8:622
3. Yin LX, Liebscher J (2007) Chem Rev 107:133

4. Kyotani T (2000) Carbon 38:269
5. Lee J, Kim J, Hyeon T (2006) Adv Mater 18:2073
6. Yang H, Zhao DY (2005) J Mater Chem 15:1217
7. Tiemann M (2008) Chem Mater 20:961
8. Ryoo R, Joo SH, Kruk M, Jaroniec M (2001) Adv Mater 13:677
9. Wan Y, Yang HF, Zhao DY (2006) Acc Chem Res 39:423
10. Lu AH, Schuth F (2006) Adv Mater 18:1793
11. Liang CD, Hong KL, Guiochon GA, Mays JW, Dai S (2004) Angew Chem Int Ed 43:5785
12. Tanaka S, Nishiyama N, Egashira Y, Ueyama K (2005) Chem Commun 212:5
13. Meng Y, Gu D, Zhang FQ, Shi YF, Yang HF, Li Z, Yu CZ, Tu B, Zhao DY (2005) Angew Chem Int Ed 44:7053
14. Wan Y, Qian XF, Jia NQ, Wang ZY, Li HX, Zhao DY (2008) Chem Mater 20:1012
15. Wan Y, Shi YF, Zhao DY (2008) Chem Mater 20:932
16. Hassan J, Sevignon M, Gozzi C, Schulz E, Lemaire M (2002) Chem Rev 102:1359
17. Venkatraman S, Li CJ (1999) Org Lett 1:1133
18. Mukhopadhyay S, Rothenberg G, Gitis D, Sasson Y (2000) Org Lett 2:211
19. Polshettiwar V, Molnar A (2007) Tetrahedron 63:6949
20. Davies IW, Matty L, Hughes DL, Reider PJ (2001) J Am Chem Soc 123:10139
21. Li CJ (2005) Chem Rev 105:3095
22. Wu XF, Li XH, Zanotti-Gerosa A, Pettman A, Liu JK, Mills AJ, Xiao JL (2008) Chem Eur J 14:2209
23. Wu XF, Liu JK, Li XH, Zanotti-Gerosa A, Hancock F, Vinci D, Ruan JW, Xiao JL (2006) Angew Chem Int Ed 45:6718
24. Narayan S, Muldoon J, Finn MG, Fokin VV, Kolb HC, Sharpless KB (2005) Angew Chem Int Ed 44:3275
25. Baleizao C, Corma A, Garcia H, Leyva A (2004) J Org Chem 69:439
26. Corma A, Das D, Garcia H, Leyva A (2005) J Catal 229:322
27. Grushin VV, Alper H (1994) Chem Rev 94:1047
28. Hassan J, Hathroubi C, Gozzi C, Lemaire M (2001) Tetrahedron 57:7845
29. Liu RL, Shi YF, Wan Y, Meng Y, Zhang FQ, Gu D, Chen ZX, Tu B, Zhao DY (2006) J Am Chem Soc 128:11652
30. Wang SY, Moon SH, Vannice MA (1981) J Catal 71:167
31. Zhao DY, Huo QS, Feng JL, Stucky GD (1998) J Am Chem Soc 120:6024
32. Meng Y, Gu D, Zhang FQ, Shi YF, Cheng L, Feng D, Wu ZX, Chen ZX, Wan Y, Stein A, Zhao DY (2006) Chem Mater 18:4447
33. Thomas AC (1975) In: Photoelectron and auger spectroscopy, 1st edn. Plenum, New York
34. Wu YY, Livneh T, Zhang YX, Cheng GS, Wang JF, Tang J, Moskovits M, Stucky GD (2004) Nano Lett 4:2337
35. Wan Y, Wang HY, Zhao QF, Klingstedt M, Terasaki O, Zhao DY (2009) J Am Chem Soc 131:4541
36. Zhuang X, Wan Y, Feng CM, Shen Y, Zhao DY (2009) Chem Mater 21:706
37. Wan Y, Zhang DQ, Zhai YP, Feng CM, Chen J, Li HX (2007) Chem Asian J 2:875
38. Wan Y, Chen J, Zhang DQ, Li HX (2006) J Mol Catal A: Chem 258:89
39. Gomez-Quero S, Cardenas-Lizana F, Keane MA (2008) Ind Eng Chem Res 47:6841